



**HAL**  
open science

# Assembled pentasil nanosheet zeolites: Adjusting the sheet thickness through a simple and direct dual templating approach

Shadi Al-Nahari, Bruno Alonso

## ► To cite this version:

Shadi Al-Nahari, Bruno Alonso. Assembled pentasil nanosheet zeolites: Adjusting the sheet thickness through a simple and direct dual templating approach. *Microporous and Mesoporous Materials*, 2024, 372, pp.113093. 10.1016/j.micromeso.2024.113093 . hal-04524708

**HAL Id: hal-04524708**

**<https://hal.science/hal-04524708>**

Submitted on 28 Mar 2024

**HAL** is a multi-disciplinary open access archive for the deposit and dissemination of scientific research documents, whether they are published or not. The documents may come from teaching and research institutions in France or abroad, or from public or private research centers.

L'archive ouverte pluridisciplinaire **HAL**, est destinée au dépôt et à la diffusion de documents scientifiques de niveau recherche, publiés ou non, émanant des établissements d'enseignement et de recherche français ou étrangers, des laboratoires publics ou privés.

# Assembled pentasil nanosheet zeolites: adjusting the sheet thickness through a simple and direct dual templating approach

Shadi Al-Nahari\* and Bruno Alonso\*

ICGM, Université de Montpellier, CNRS, ENSCM, 34293 Montpellier cedex 5, France.

E-mail: [bruno.alonso@enscm.fr](mailto:bruno.alonso@enscm.fr)

**A one-step synthesis method allows tuning the silicalite nanosheets' thickness from 2 to 30 nm in self-pillared zeolites. The adjustment is achieved by mixing two simple organic structure-directing agents (OSDAs): tetrapropylammonium (TPA) and tetrabutylammonium (TBA). The proportion of incorporated TBA, known to favour silicalite nanosheets, determines the morphological variations observed.**

A breakthrough in zeolites' development is the synthesis of hierarchical zeolites in the form of assembled crystalline sheets of nanometre dimensions (< 100 nm).<sup>1</sup> For catalysis applications notably, these materials could offer superior advantages in terms of reducing diffusion lengths and coke formation. In the case of silicalite zeolites (MFI and MEL frameworks), the approaches deal with tuning the crystallization and/or MFI/MEL intergrowth rates mostly with the use of organic structure directing agents (OSDAs). This can be achieved by: i) stopping crystal growth in the b direction by introducing long hydrophobic alkyl chains bound to diquateryammoniums (diquats),<sup>2</sup> ii) using OSDAs with long chains acting as surfactants,<sup>3</sup> iii) favouring rotational intergrowth to form self-pillared pentasil (SPP) layers with OSDAs such as small diquats,<sup>4</sup> tetrabutylphosphonium (TBP) or tetrabutylammonium (TBA).<sup>5</sup> The latter is one of the simplest methods of synthesizing zeolitic nanosheets that involves employing the commercially available TBA-OH as OSDA. It results in the formation of SPP nanosheets with a house-of-cards structure, comprised of MFI/MEL intergrowth, as demonstrated by Tzapatsis *et al.*<sup>5</sup> More recently, Han *et al.* used both tetrapropylammonium (TPA) and TBA commercial OSDAs to yield the same type of zeolites but consisting of the MFI-phase.<sup>6</sup>

Modulation of the nanosheets' thickness, an important issue for applications, has been demonstrated for some of the above systems by varying the type of multi-quaternaryammonium surfactants or their relative quantity in sols of varied compositions,<sup>7</sup> or by using additional post-synthetic treatments like steam coarsening.<sup>8</sup>

Here, we take a step further and demonstrate how assembled zeolitic nanosheets with controllable thicknesses can be easily obtained using a dual templating method involving commercially available OSDAs in a simple single-step synthesis.

We synthesized the different zeolite particles by varying only the TPA-TBA proportions without any use of additional cations (details in ESI). SEM and TEM images revealed that the as-synthesized samples are composed of homogenous single-population particles (**Fig. S1** and **S2**, ESI). The particle sizes were also measured which either correspond to near spherical nanoparticles in the case of only TPA templating or stacked sheets forming a 3D house-of-card particle as the case with TBA and dual templating. Interestingly, the particle sizes increase from 90 to ca. 270 nm with increasing the TBA % (**Fig. S3**, ESI). It was also evident that there is a progressive thickening of the sheets as we started introducing TPA (and decreasing TBA %). We found that in the range of 90-100 % initial TBA, the sheet thickness can be varied from a single-unit-cell of MFI or MEL (ca. 2 nm) up to ca. 30 nm (**Fig. 1** and **S5**, ESI). These results are remarkable, as they also show a gradual and almost linear relationship between nanosheets thickness and TBA % (initial as well as final, *vide infra*).

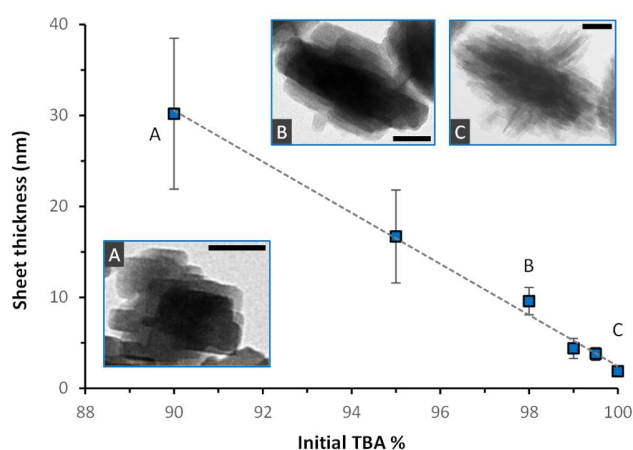


**Fig. 1** Nanosheets' thickness as a function of initial TBA %. Errors bars correspond to  $\pm$  standard deviations. The dashed line is a linear fit regression ( $y = -2.81x + 283.35$ ,  $R^2 > 0.99$ ). The onsets correspond to TEM images of particles suspensions for: (A) 90, (B) 98 and (C) 100 % of initial TBA. The scale bars are 50 nm.

The XRD patterns of all zeolites in Fig. 2 confirm the crystallinity observed by TEM (**Fig. S6**, ESI). When using only TPA as the OSDA, we obtain a pure MFI phase as expected. However, as we gradually introduce TBA into the synthetic mixture, the XRD peaks that are unique to the MFI structure decrease in intensity. This is the case for the peaks at ca.  $23.7^\circ$  and  $24.4^\circ$  corresponding to the (151) and (313) (133) MFI crystallographic planes respectively, not present in MEL structures (**Fig. 2**). In addition, the peak at approx.  $45^\circ$  appears as a single peak when using TBA, which has been described as indicative of the MEL phase.<sup>9</sup> In contrast, when using TPA, the same peak appears as a symmetric doublet, indicating the MFI phase.<sup>9,10</sup>

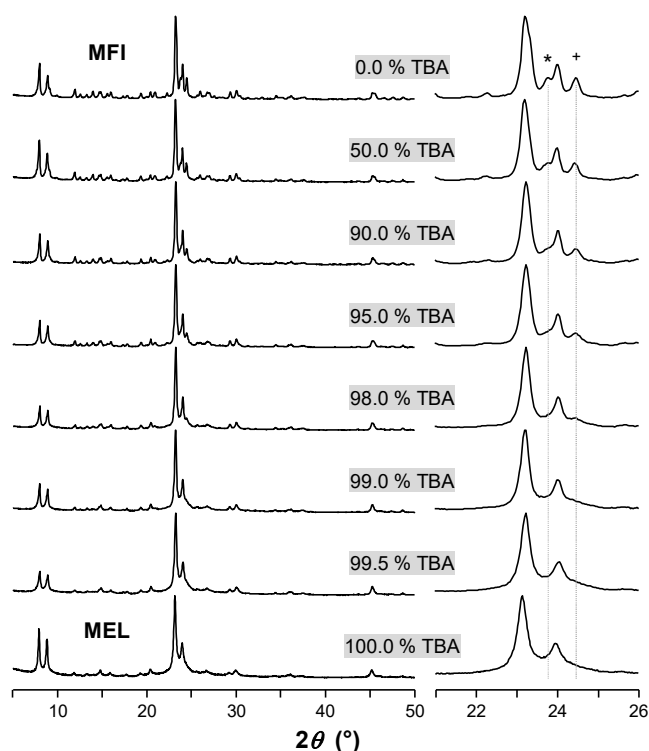


**Fig. 2** XRD patterns of as-synthesized silicalite zeolites synthesized using different initial proportions of TPA and TBA. A zoomed view on the XRD patterns between 21 and 26  $2\theta$  degrees is presented on the right side. Peaks assigned with \* and + correspond to the MFI crystallographic planes (151), and (313) and (133), respectively.

Based on these characteristics MEL diffractions,<sup>11</sup> we propose that when only TBA is used, the final material is at least primarily composed of MEL with possible MFI intergrowth which also aligns with recent findings.<sup>6</sup> Also, Long *et al.*, who first reported this synthetic method with TBA, described their materials as "aggregates of plate-like or needle-like particles" and identified them as MEL phase.<sup>12</sup>

Through careful analysis, we observed a progressive broadening of the XRD peaks as TBA % is increased. This is the case for instance for the first peak at around 7.9°, corresponding to (101) in MEL and (101) and (011) in MFI (**Fig. S7A**, ESI). While this observation aligns well with the hypothesis of thinning sheets, it could also be due to evolvments in the crystal structure such as an increase in stacking faults of MFI/MEL intergrowth.<sup>13</sup> Besides, a similar evolution of the FWHM up to 98 % of initial TBA is also presented for peaks reserved only for the MFI structure like that at ca. 24.4° (**Fig. S7B**, ESI). These results indicate a global evolution in the structure of the samples as we gradually transition from MFI to MEL. Such a gradual evolution also affects the local geometry of the silicalite frameworks as noticed from the minute variations in <sup>29</sup>Si NMR spectra with TBA % (**Fig. S8**, ESI).

We collected <sup>13</sup>C{<sup>1</sup>H} CP-MAS NMR spectra to verify the incorporation of both OSDAs. From **Fig. 3**, we observe that introducing initially the OSDA as 100 % TPA or as equal molar amounts of TBA and TPA (50 % TBA) yields identical <sup>13</sup>C spectra corresponding only to TPA in MFI. This means that when introducing both OSDAs in equal amounts, and in excess with respect to Si, only TPA is favoured as the primary director of the zeolite structure. The preference for TPA in the crystallization has also been documented in literature.<sup>6,13</sup> This is also in agreement with previous calculations on the interaction and stabilization energies of the MFI or MEL zeolites occluding TPA or TBA.<sup>14</sup> The <sup>13</sup>C NMR spectrum of the 100 % TBA sample presented peaks resembling to those published in literature for TBA occluded in MEL.<sup>12</sup>

When the TPA is introduced in scarce quantities – initial TBA ≥ 90 % – <sup>13</sup>C NMR shows the presence of both TBA and TPA cations in the zeolite (**Fig. 3**). <sup>13</sup>C NMR spectra also show that the peaks associated with TPA and TBA do not retain their exact chemical shift positions when compared to pure TPA or TBA in MFI. These spectral observations suggest that the environment of one OSDA is modified by the presence of the other OSDA and/or the evolution in the hosting environment. Therefore, our synthesized materials do not consist of heterogeneous mixtures of two distinct zeolite populations (one with TPA exclusively and another with TBA). Rather, these changes in the <sup>13</sup>C chemical shifts of TPA or TBA peaks illustrate a mutual effect due to the presence of both OSDAs in the same zeolite. The <sup>13</sup>C spectra are also similar to those obtained by Tuel and Taârit<sup>15</sup> for their synthesis of Ti-containing MFI/MEL samples using TBA/TPA OSDA mixtures, where they described obtaining homogeneous samples.

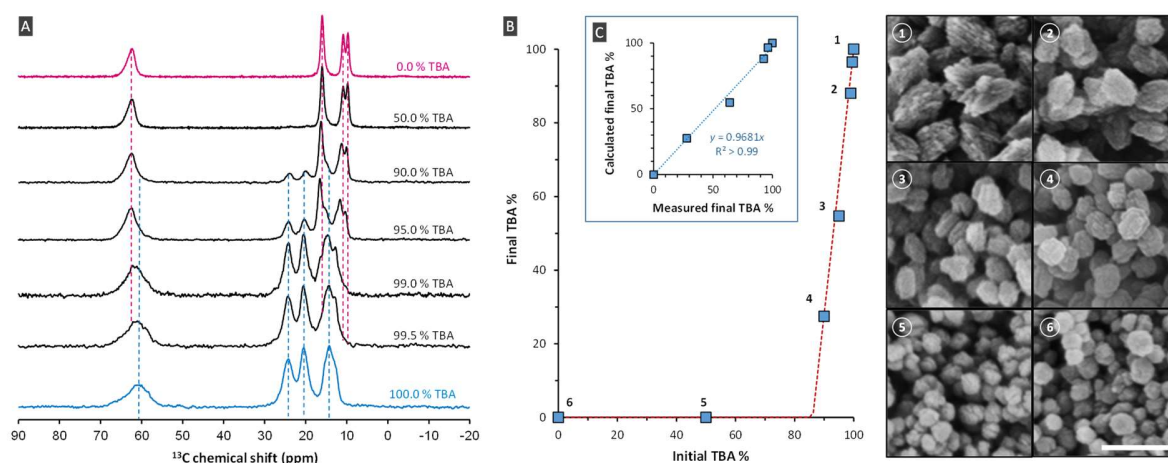


**Fig. 3** (A)  $^{13}\text{C}\{^1\text{H}\}$  CP-MAS NMR spectra ( $\nu_0[^{13}\text{C}] = 75.5$  MHz,  $\nu_{\text{MAS}} = 5$  kHz) of as-synthesized silicalite zeolites. Si:OSDA molar ratio is 1:0.3 with the OSDA being composed of TPA and TBA cations introduced in different molar percentages. The TBA percentages listed are the initial in the synthetic mixture. (B) Final TBA % as a function of initial TBA %. The squares correspond to measured values from the deconvolution of  $^{13}\text{C}\{^1\text{H}\}$  single pulse NMR spectra. The red dotted line is calculated considering that all TPA present in the initial mixture is first up taken in the samples. The numbers refer to the SEM images on the right (scale bar is 300 nm). (C) Calculated final TBA % values as a function of measured final TBA %. The dotted line represents a linear fit between these values.

In order to quantify the TPA/TBA percentages in the final obtained material, we recorded single-pulse quantitative  $^{13}\text{C}$  NMR spectra (Fig. S9, ESI). By fitting these spectra, it is possible to evaluate the relative quantity of the incorporated TBA (Table S2, ESI). The obtained results are consistent with the variations observed for  $^1\text{H}$  NMR spectra recorded at very high magnetic field (20 T) and MAS frequencies (100 kHz) presenting an improved spectrum resolution (Fig. S10-S11, ESI). It is noteworthy that after a threshold, the percentage of the incorporated TBA increases almost linearly with the initial % of TBA (Fig. 3B). Interestingly, these estimated final TBA % based on  $^{13}\text{C}$  fits exhibit a linear correlation with the calculated values for the final TBA % (Fig. 3C). The calculated values are obtained here making the hypothesis that all the TPA in the reacting medium is preferentially consumed and incorporated into the MFI zeolite. So, any remaining TPA vacancies are occupied by TBA since TPA is fully consumed. This hypothesis, confirmed by the correlation found above, can also agree with the putative mechanism of formation proposed by Han *et al.* for TPA-TBA zeolites (94 % TBA) where TPA substitutes a maximum of TBA molecules during a recrystallization step.<sup>6</sup> Here we show that this preferential uptake of TPA is common to all OSDA compositions.

The samples present slight differences in their TGA profiles and in their weight loss percentages that correspond to the OSDA quantity (Fig. S12A, ESI). The TG peaks associated with OSDA decomposition exhibit variability in their temperatures depending on the OSDA mixture percentages (Fig. S12B, ESI). This indicates a difference in the stability of the OSDA within the material that can be linked to the structural variation of the formed material. It is also noteworthy that the highest increases in decomposition temperatures observed for both OSDAs are in the sample presenting similar final quantities of the OSDAs (initial 95 % of TBA, and final  $\approx 55$  % of TBA).

Variations in the decomposition temperatures of the OSDAs - when used as dual templates in comparison to when using them alone - were also demonstrated in a study by Blasco *et al.*, where they employed dual templating for bulk MFI zeolites.<sup>16</sup> The authors explain that this observation suggests the coexistence of the “two organic agents as an intimate mixture filling the pores of the MFI”. Herein, our findings further support the conclusions drawn from  $^{13}\text{C}$  NMR analysis, suggesting that rather than forming two heterogeneous mixtures of materials, a single structure is formed with the extent of modification dependent on the introduced OSDA percentages. The morphological variations observed - in particle sizes, aspect ratio and nanosheets' thickness -

strictly depend here on the quantity of TBA incorporated in the final zeolite particles (**Fig. S13**, ESI). Notably, the nanosheets' thickness is found to be proportional to the final TBA %.

From TEM analysis, the nanosheet morphology is still present in the calcined zeolites (**Fig. S14**, ESI) and crystalline domains are maintained within the nanosheets (**Fig. S15**, ESI). However, we observe some differences between samples. For the zeolite synthesized with 100 % TBA, the nanosheets seem more condensed losing their distinct separation. On the other hand, the sample synthesized with 99 % TBA appears less affected by the calcination step.

All calcined zeolites present indeed the typical XRD patterns of porous silicalite (MFI, MEL) (**Fig. S16**, ESI). And the gradual broadening of the peaks when TBA % increases is also observed (**Fig. S17**, ESI). N<sub>2</sub> sorption isotherms (**Fig. S18**, ESI) resemble to that published for SPP zeolites.<sup>6</sup> With the present dual templating approach, a similar amount of microporosity is preserved over the samples ( $V_{microp.}$  in the 0.12-0.17 cm<sup>3</sup>.g<sup>-1</sup> range). The zeolites synthesized exhibited noticeable hysteresis loops for  $p/p_0 \geq 0.9$  indicative of capillary condensation. This is pointing to the presence of mesoporosity coming from the arrangement of external zeolites surfaces in addition to mesoporosity created by particle aggregation. The estimated mesopore sizes are in the range 20-40 nm (**Fig. S19**, ESI). The zeolite synthesized with 100 % TBA differs from the others. The partial collapse of nanosheets noticed for this particular sample is decreasing the available mesoporosity. This is not observed for SPP zeolites previously synthesized with TBP<sup>5</sup> or a TPA/TBA mixture,<sup>6</sup> and for all the other zeolites here.

Given the significance of Al-containing zeolites in catalytic applications, it is important to verify whether their synthesis is successful with the OSDAs mixtures. It is worth noting that there are only small morphological differences observed between the pure-silica and Al-containing zeolites (**Tables S2** and **S3** respectively, ESI). No major differences are observed for XRD patterns and <sup>13</sup>C NMR spectra recorded with or without Al when using the same TBA % in the OSDA mixture (**Fig. S20-S21**, ESI). Therefore, the general trend concerning the particle sizes and sheet thickness remains valid for the Al-containing samples.

For these zeolites, <sup>27</sup>Al NMR spectra show main peaks around 50-60 ppm corresponding to the tetrahedral Al<sup>IV</sup> atoms inside the zeolite framework. We also notice the presence of small peaks in the range of 0-10 ppm corresponding to extra-framework (six-coordinated) Al<sup>VI</sup>, as observed previously in such type of materials.<sup>5,6</sup> The shape and the width of the Al<sup>IV</sup> peaks vary with the initial % of TBA. This indicates different local environments for the Al sites. For the zeolite made only with TBA, Al<sup>IV</sup> sites are located at the surface or in the core of very thin pentasil sheets (*ca.* 2 nm thick) possessing a high degree of geometrical disorder due to the deformations induced by the external surface and possibly also the vicinity of the bulkier OSDA TBA. On the contrary, in the zeolites made only with TPA, Al sites are located inside bigger crystalline domains, much less subjected to the influence of the external surface. We have made a rough fit of the related <sup>27</sup>Al peaks of both 100 and 0 % TBA zeolites with a single Gaussian line (**Fig. 4**). These Gaussian fits allow to keep the information on the peaks' positions and widths. Using a linear combination of the two Gaussian lines obtained, it becomes possible to fit with reasonably good accuracy the <sup>27</sup>Al peak for Al<sup>IV</sup> sites in the 99 % TBA sample. From this fit, we might thus hypothesize that about 58 % of the Al sites in this zeolite are located in positions strongly influenced by the external surface.

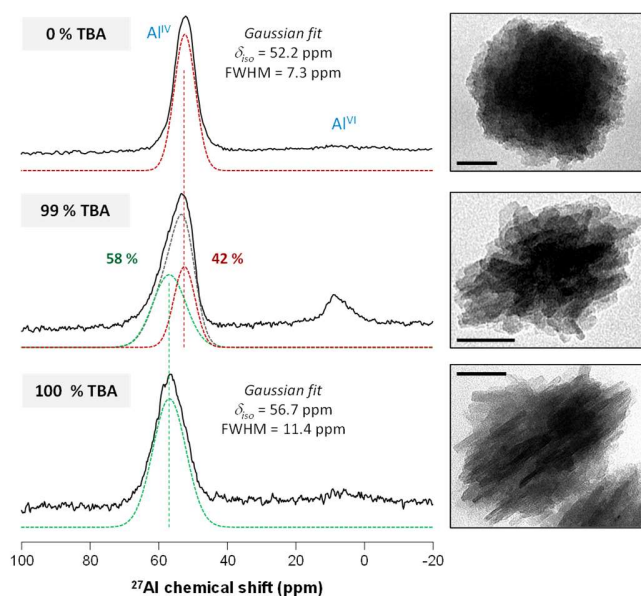


**Fig. 4**  $^{27}\text{Al}$  NMR spectra of as-synthesized Al containing zeolites of different initial TBA %. The spectra of 0 and 100 % TBA samples are fitted using Gaussian functions. The spectrum of the 99 % TBA sample is fitted by only varying the amplitude of the two obtained Gaussian functions. The percentages correspond to the resulting signal area proportions. TEM images on the right are representative of the zeolites analyzed on the left. The scale bars are 50 nm.

In conclusion, the proportion of TBA incorporated in the final zeolite particles directly determines their morphological and structural properties. The dual templating method presented here offers thus a straightforward approach for synthesizing SPP zeolites with gradual control of the nanosheets' thickness in the 2-30 nm range by adjusting the initial TBA %. With an excess of both TPA and TBA, there is a preferential uptake of TPA for all the composition range explored, and the proportion of incorporated TBA can be deduced accordingly. This simple method allows the incorporation of Al into different environments opening additional perspectives for catalytic applications.

We acknowledge the specific financial support for this work from the French National Research Agency (project ZEOORG ANR-19-CE29-0008) and the CNRS for the access to the high magnetic field through the Infranalytics facility (FR-2054). We further thank for their support at the local facilities: XRD (D. Granier), TEM (F. Godiard), SEM (B. Rebière), SSNMR (V. Sarou-Kanian, P. Gaveau, E. Fernandez), TGA (C. Biolley, N. Donzel), XRF (J. Fullenwarth).

## References

- 1 M. Shamzhy, B. Gil, M. Opanasenko, W. J. Roth and J. Čejka, *ACS Catal.*, 2021, 11, 2366; X. Wang, Y. Ma, Q. Wu, Y. Wen and F.-S. Xiao, *Chem. Soc. Rev.*, 2022, 51, 2431.
- 2 M. Choi, K. Na, J. Kim, Y. Sakamoto, O. Terasaki and R. Ryoo, *Nature*, 2009, 461, 246; K. Na, M. Choi, W. Park, Y. Sakamoto, O. Terasaki and R. Ryoo, *J. Am. Chem. Soc.*, 2010, 132, 4169.
- 3 L. Meng, B. Mezari, M. G. Goesten and E. J. M. Hensen, *Chem. Mater.*, 2017, 29, 4091; L. Meng, X. Zhu, W. Wannapakdee, R. Pestman, M. G. Goesten, L. Gao, A.J.F. van Hoof and E. J. M. Hensen, *J. Catal.*, 2018, 361, 135.
- 4 W. Chaikittisilp, Y. Suzuki, R.R. Mukti, T. Suzuki, K. Sugita, K. Itabashi, A. Shimojima and T. Okubo, *Angew. Chem. Int. Ed.*, 2013, 52, 3355.
- 5 X. Zhang, D. Liu, D. Xu, S. Asahina, K. A. Cychosz, K. V. Agrawal, Y. Al Wahedi, A. Bhan, S. Al Hashimi, O. Terasaki, M. Thommes and M. Tsapatsis, *Science*, 2012, 336, 1684.
- 6 X. Zhao, S. Zeng, X. Zhang, Q. Deng, X. Li, W. Yu, K. Zhu, S. Xu, J. Liu and L. Han, *Angew. Chem. Int. Ed.*, 2021, 60, 13959.
- 7 W. Park, D. Yu, K. Na, K. E. Jelfs, B. Slater, Y. Sakamoto and R. Ryoo, *Chem. Mater.*, 2011, 23, 5131; Y. Kim, K. Kim and R. Ryoo, *Chem. Mater.*, 2017, 29, 4, 1752; F. Feng, L. Wang, X. Zhang and Q. Wang, *Ind. Eng. Chem. Res.*, 2019, 58, 5432.
- 8 Y. Guefrachi, G. Sharma, D. Xu, G. Kumar, K.P. Vinter, O. A. Abdelrahman, X. Li, S. Alhassan, P. J. Dauenhauer, A. Navrotsky, W. Zhang and M. Tsapatsis, *Angew. Chem. Int. Ed.*, 2020, 59, 9579.
- 9 A. Tuel, Y. Ben Taarit and C. Naccache, *Zeolites*, 1993, 13, 454.
- 10 G. A. Jablonski, L.B. Sand and J.A. Gard, *Zeolites*, 1986, 6, 396.
- 11 D.M. Bibby, N.B. Milestone and L.P. Aldridge, *Nature*, 1979, 280, 664.
- 12 J. Dong, J. Zou and Y. Long, *Microporous Mesoporous Mater.*, 2003, 57, 9.
- 13 G. Perego, G. Bellussi, A. Carati, R. Millini and V. Fattore, in *Zeolite Synthesis*, ed. M.L. Occelli Mario and H. E. Robson, ACS Symposium series 398, Washington DC, 1989, ch. 25, 360-373.
- 14 V. Shen and A. T. Bell, *Microporous Mater.*, 1996, 7, 187; E. de Vos Burchart, H. van Koningsveld and B. van de Graaf, *Microporous Mater.*, 1997, 8, 215; M. Sánchez, R. D. Díaz, T. Córdova, G. González and F. Ruetter, *Microporous Mesoporous Mater.*, 2015, 203, 91.
- 15 A. Tuel and Y. Ben Taarit, *Zeolites*, 1994, 14, 169.
- 16 J. Martinez-Ortigosa, J. Simancas, J. A. Vidal-Moya, P. Gaveau, F. Rey, B. Alonso and T. Blasco, *J. Phys. Chem. C*, 2019, 123, 22324.

- Electronic Supplementary Information (ESI) -

**Self-pillared pentasil zeolites: adjusting the thickness of nanosheets  
through a simple and direct dual templating approach**

Shadi Al-Nahari and Bruno Alonso

ICGM, Université de Montpellier, CNRS, ENSCM, 34293 Montpellier cedex 5, France

## Table of Contents

<b>1. Synthesis of zeolite nanosheets .....</b>	<b>9</b>
<b>2. Characterisation techniques .....</b>	<b>10</b>
<b>3. Solid-State NMR experiments .....</b>	<b>11</b>
<b>4. Additional characterisation data .....</b>	<b>12</b>
<b>5. Additional data on calcined zeolites .....</b>	<b>22</b>
<b>6. Additional data for the Al-containing zeolites .....</b>	<b>25</b>
<b>7. ESI References .....</b>	<b>26</b>

# 1. Synthesis of zeolite nanosheets

## Chemicals

Tetraethyl orthosilicate (TEOS) ( $\text{SiC}_8\text{H}_{20}\text{O}_4$ , Aldrich,  $\geq 99\%$ ), tetra-n-propylammonium hydroxide (TPAOH) ( $\text{C}_{12}\text{H}_{28}\text{OHN}$ , Thermo Scientific, 40 % w/w aq. soln.), tetrabutylammonium hydroxide (TBAOH) ( $\text{C}_{16}\text{H}_{37}\text{ON}$ , Sigma-Aldrich, 40 % w/w aq. soln.), aluminum isopropoxide ( $\text{C}_9\text{H}_{21}\text{O}_3\text{Al}$ , Aldrich,  $\geq 98\%$ ), demineralized water was obtained from exchange resins.

## Method

The synthesis protocol for the materials was adapted from literature.<sup>1</sup> The initial molar ratios were as follows:  $1\text{SiO}_2:0.3\text{OSDA}:10\text{H}_2\text{O}:4\text{EtOH}$ . The OSDA (in solution in its hydroxide form, 40 % w/w aq) was added dropwise into TEOS (0.06 moles) while stirring followed by the addition of the rest of demineralized water. The solution was stirred for 14 h while covered then transferred to a Teflon-lined PTFE chamber sealed with a stainless-steel autoclave to start the thermal treatment at 388 K. The thermal treatment duration was 40 h. The product was centrifuged several times to separate and wash the product until the pH of the supernatant is lower than 9. Each centrifugation cycle lasted for 10 min with 20,000 rpm speed. The product was then dried at 353 K overnight.

## Synthesis of silicalite zeolites containing TPA/TBA mixtures

The same synthesis method described above was used with the OSDA being both TPAOH and TBAOH added consecutively to TEOS. To yield nanosheets with varying thicknesses, we varied the molar percentages of the OSDA. For instance, a sample with 99 % TBA and 1 % TPA corresponds to the following molar ratios:  $1\text{SiO}_2:0.297\text{TBA}:0.003\text{TPA}:10\text{H}_2\text{O}$  where the sum of the molar ratios of the OSDAs corresponds to 0.3. The synthesized samples are listed below (**Table S1**). Yields estimated from dried powders are  $61 \pm 8$  molar %.

**Table S1** Silicalite samples synthesized with the OSDA being a different mixture of TPA and TBA. The TBA % corresponds to the molar % of TBA used as an OSDA in the synthetic mixture. Yields are estimated from dried samples' weights.

<b>Initial TBA (%)</b>	100	99.5	99	98	95	90	50	0
<b>Yield (%)</b>	51	64	67	66	72	75	73	76

## Al-containing zeolites

The Al-containing zeolites were synthesized following the same above-mentioned protocols and without the addition of  $\text{Na}^+$ . We added the aluminum isopropoxide to TEOS prior to the addition of the OSDA. The initial Si/Al molar ratio in the solution was 100. Final Si/Al values are between 39 and 75 as measured by XRF (**Table S3**).

## Calcination

The porous zeolites were obtained by calcination at 823 K for 8 h under air with a ramp rate of  $2 \text{ K}\cdot\text{min}^{-1}$ .

## 2. Characterisation techniques

### **Powder X-ray diffraction**

Powder X-ray diffraction patterns (PXRD) were collected using Bragg Brentano geometry with Bruker AXS D8 diffractometer using Cu K $\alpha$  radiation (1.5406 Å wavelength). The diffractometer measured the peaks with an angle ( $2\theta$ ) range from 5° to 60° and a step size of 0.033.

### **Thermogravimetric analysis**

Thermogravimetric analysis (TGA) was done using NETZSCH TG 209 with alumina crucibles from 313 to 1173 K at a 10 K.min<sup>-1</sup> heating rate under air.

### **Scanning Electron Microscopy**

Scanning Electron Microscopy (SEM) images were collected with a HITACHI 4800 S microscope using platinum coating on the samples (< 50 Å) prior to the observation.

### **Transmission electron microscopy**

Transmission Electron Microscopy (TEM) images were collected with JEOL 1400 Flash transmission electron microscope (LaB6 microscope working at 120kV). Absolute Ethanol containing the sample powder was sonicated briefly then deposited on the TEM carbon coated grids. The grids were left to dry at room temperature for at least 12 h. Distance measurements and image manipulations were done using the *ImageJ* software.<sup>2,3</sup>

### **Si/Al molar ratio**

To determine the Si/Al molar ratio for the Al containing samples, we used X-ray fluorescence (XRF) to detect and measure the Si and Al atomic percentages. We utilized a PANalytical AXIOS Max spectrometer with an SST-mAX50 type X-ray source (RRXG platform, Montpellier). Initially, measurements were conducted on five different calcined commercial ZSM-5 zeolites with known Si/Al ratios (Si/Al=15, 25, 40, 75, 140). Using these measurements, we established a calibration curve for Si and Al quantification, which was then applied to measure the Si and Al percentages in our samples.

### **N<sub>2</sub> sorption isotherms**

N<sub>2</sub> adsorption/desorption isotherms were obtained using a Micromeritics Tristar apparatus. The measurements were recorded at a temperature of 77 K for calcined samples that were degassed at 523 K and 3·10<sup>-3</sup> Torr overnight. To inspect microporosity formation, t-plot analyses<sup>4</sup> have been undertaken using the equation of Harkins and Jura.<sup>5</sup> From the surfaces of multimolecular layers, we estimate the micropores' specific surface area and approximate volumes  $V_{microp.}$ . Pore size distributions (PSDs) were calculated with the BJH method (mesopore volume distributions)<sup>6</sup> using desorption branches and Halsey approach for the film thickness.<sup>7</sup>

### 3. Solid-State NMR experiments

#### <sup>13</sup>C NMR

<sup>13</sup>C{<sup>1</sup>H} NMR cross polarization (CP-MAS) spectra were recorded on a Varian 300 (7.0 T) spectrometer ( $\nu_0[^{13}\text{C}] = 75.5$  MHz) with 7.5 mm rotors ( $\nu_{\text{MAS}} = 5$  kHz), using 5 ms contact time, 5 s recycle delay and <sup>1</sup>H decoupling during acquisition (50 kHz nutation frequency). <sup>13</sup>C single pulse quantitative MAS NMR spectra were recorded on the same spectrometer using  $\pi/2$  flip angle pulses with 5  $\mu\text{s}$  width and 30 s recycle delays. The powder was filled in 7.5 mm rotors spun at  $\nu_{\text{MAS}} = 5$  kHz. The number of scans was typically 2000.

Adamantane was used as an external secondary <sup>13</sup>C reference ( $\delta = 38.5$  ppm for the high frequency peak, with respect to  $\delta(\text{TMS}) = 0$  ppm).

#### <sup>29</sup>Si NMR

<sup>29</sup>Si{<sup>1</sup>H} NMR cross polarization (CP-MAS) spectra were recorded on a Varian 400 (9.4 T) spectrometer ( $\nu_0[^{29}\text{Si}] = 79.5$  MHz) with 7.5 mm rotors ( $\nu_{\text{MAS}} = 5$  kHz), using 20 ms contact time, 5 s recycle delay and <sup>1</sup>H decoupling during acquisition (50 kHz nutation frequency). Octa(dimethylsiloxy)-octasilsesquioxane (Q<sub>8</sub>M<sub>8</sub>H) was used as a secondary reference ( $\delta = -2.25$  ppm for higher frequency resonance, with respect to  $\delta(\text{TMS}) = 0$  ppm).

#### <sup>1</sup>H NMR

<sup>1</sup>H single pulse MAS NMR spectra were recorded on a Bruker spectrometer at 20.0 T ( $\nu_0(^1\text{H}) \equiv 850.0$  MHz) using  $\pi/2$  flip angle pulses with 5  $\mu\text{s}$  pulse width and recycling delays of 10 s. The rotor diameter was 0.7 mm ( $\nu_{\text{MAS}} = 100$  kHz). Chemical shifts were referenced using external references: adamantane ( $\delta = 1.8$  ppm) or TMS ( $\delta = 0$  ppm).

#### <sup>27</sup>Al NMR

<sup>27</sup>Al single pulse MAS NMR spectra were recorded at 14.1 T ( $\nu_0(^{27}\text{Al}) \equiv 156.4$  MHz) using small flip angle ( $\leq \pi/12$ ). Chemical shifts were referenced using an external Al(NO<sub>3</sub>)<sub>3</sub> 1M solution ( $\delta_{\text{iso}} = 0$  ppm).

#### Spectrum fitting

The NMR spectra were fitted using Gaussian-Lorentzian functions of the freely available *Dmfit* software.<sup>8,9</sup>

#### 4. Additional characterisation data

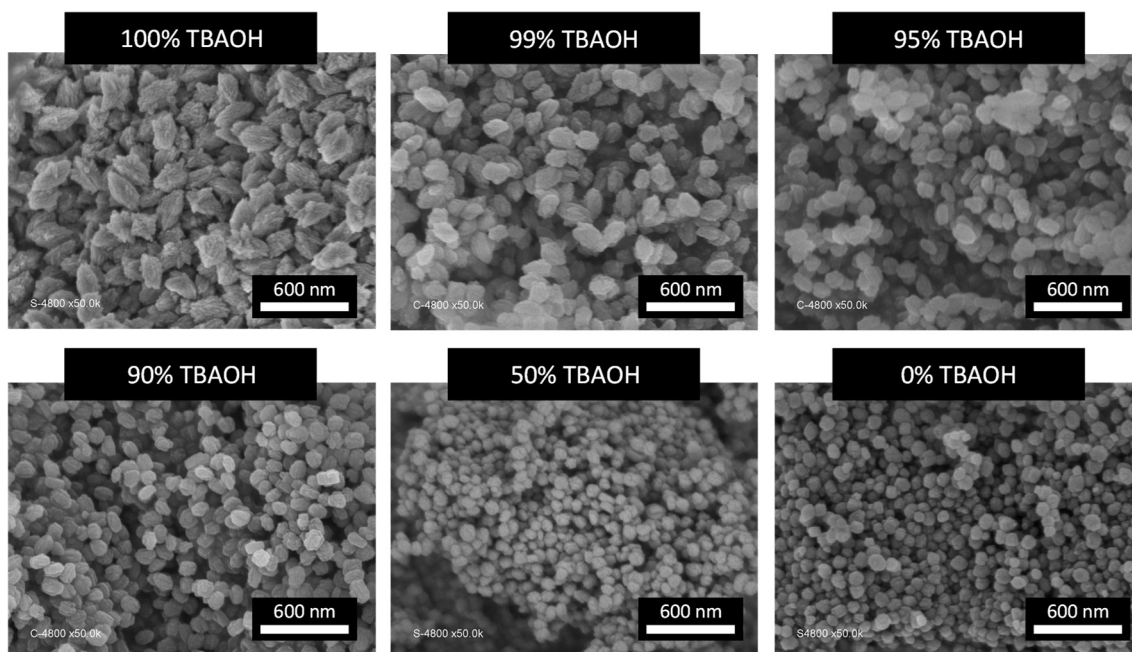


**Figure S1** SEM images of as-synthesized silicalite zeolites. ). Percentages refer to initial TBA %.

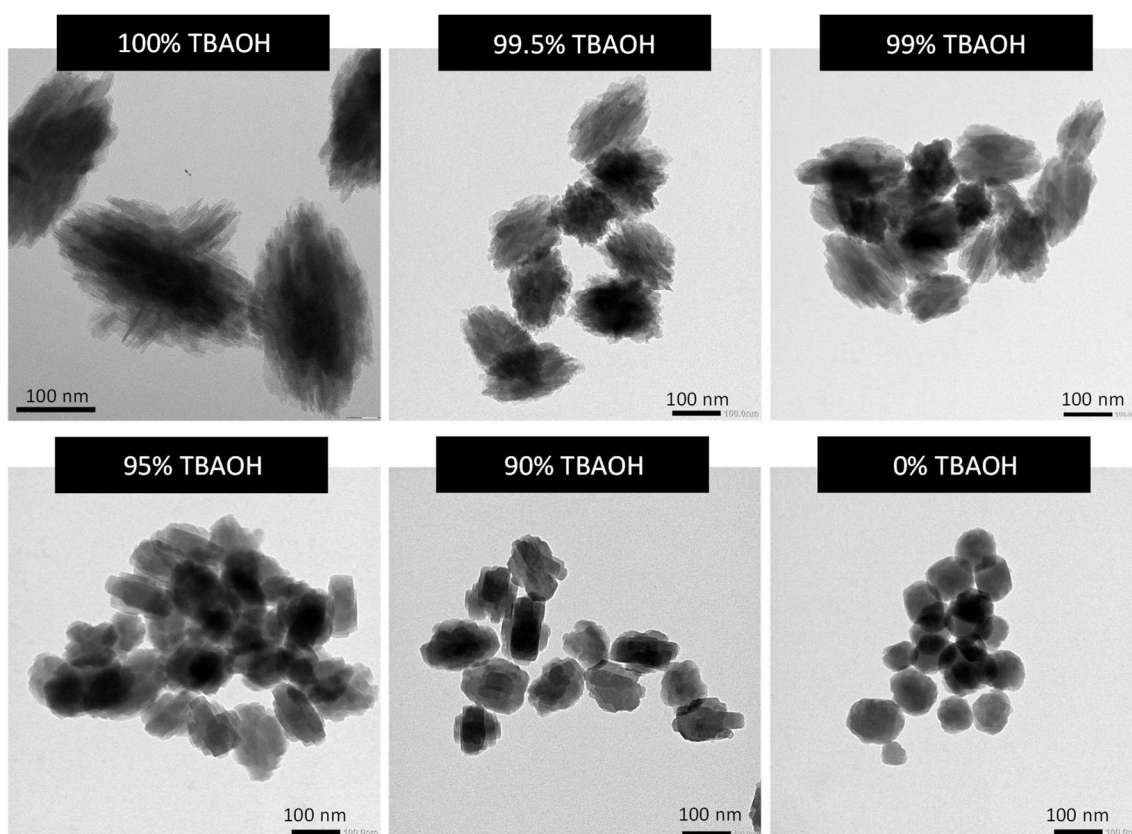


**Figure S2** TEM micrographs of as-synthesized silicalite zeolite. ). Percentages refer to initial TBA %.

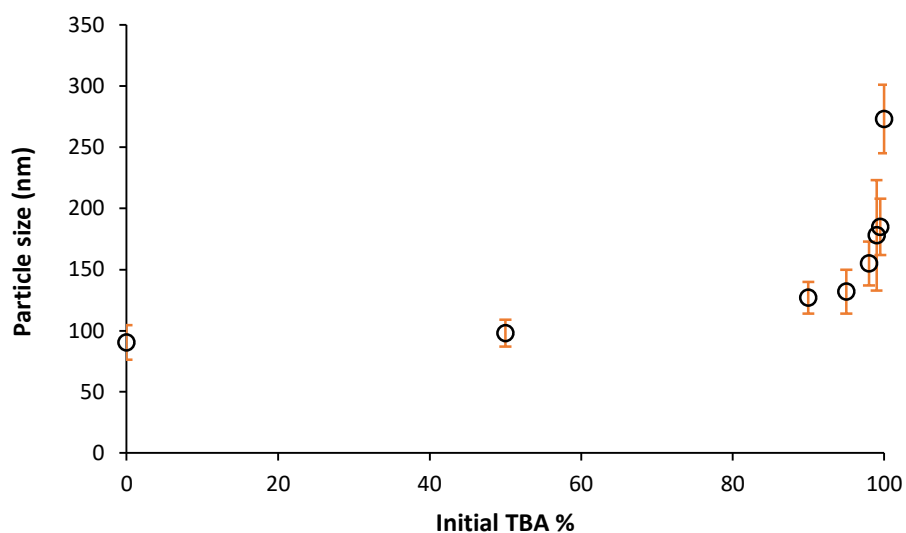


**Figure S3** Particle size of as-synthesized silicalite zeolites as a function of the initial TBA % in the OSDA synthetic mixture. Errors bars correspond to  $\pm$  standard deviations.

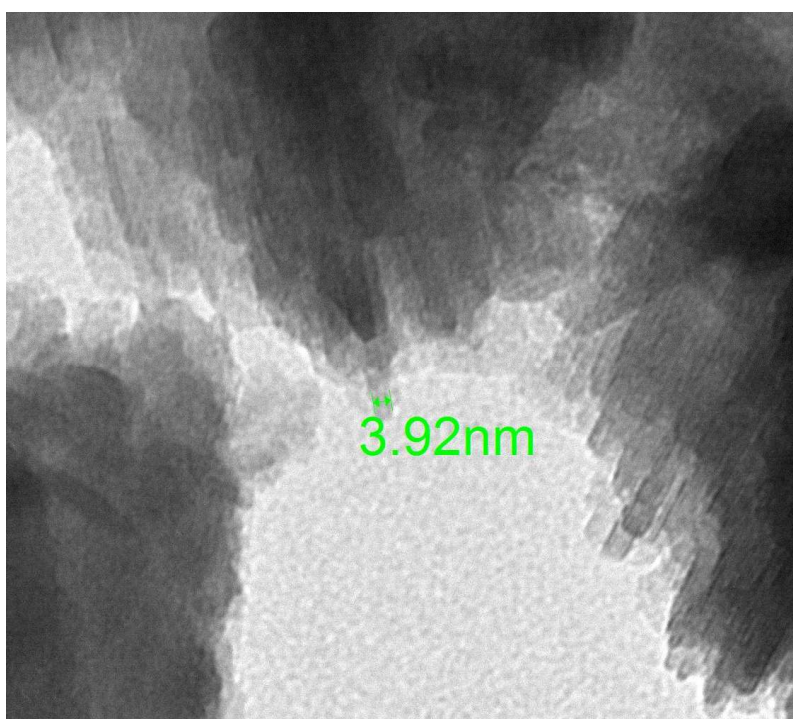


**Figure S4** Example of measuring the nanosheet thickness. Only the thinnest individual sheets were included in the measurements to prevent the inadvertent measurement of larger widths for non-perpendicular sheets. The sample in this example is 99.5 % initial TBA.

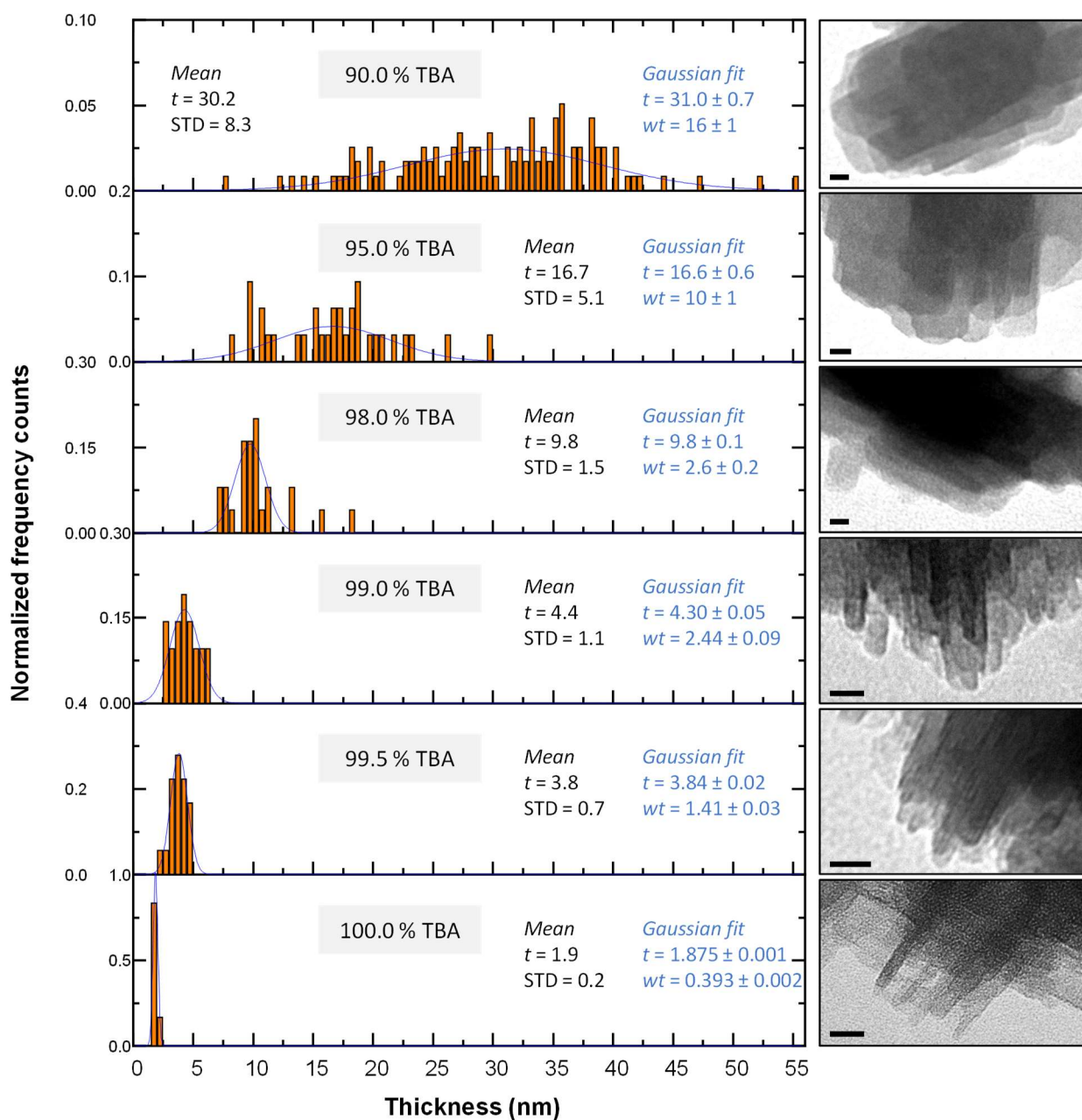


**Figure S5** Nanosheets' thickness distributions for as-synthesized silicalite zeolite of varied initial TBA %. Measured data is presented as normalized frequency counts histograms. The mean values of thickness and the related standard deviations (STD) are given in black characters. The centres and widths of Gaussian lines obtained by fitting the distributions are given in blue characters (curves in blue). All values are in nanometres. TEM images on the right are examples of micrographs considered for measurements. The scale bars are 10 nm.

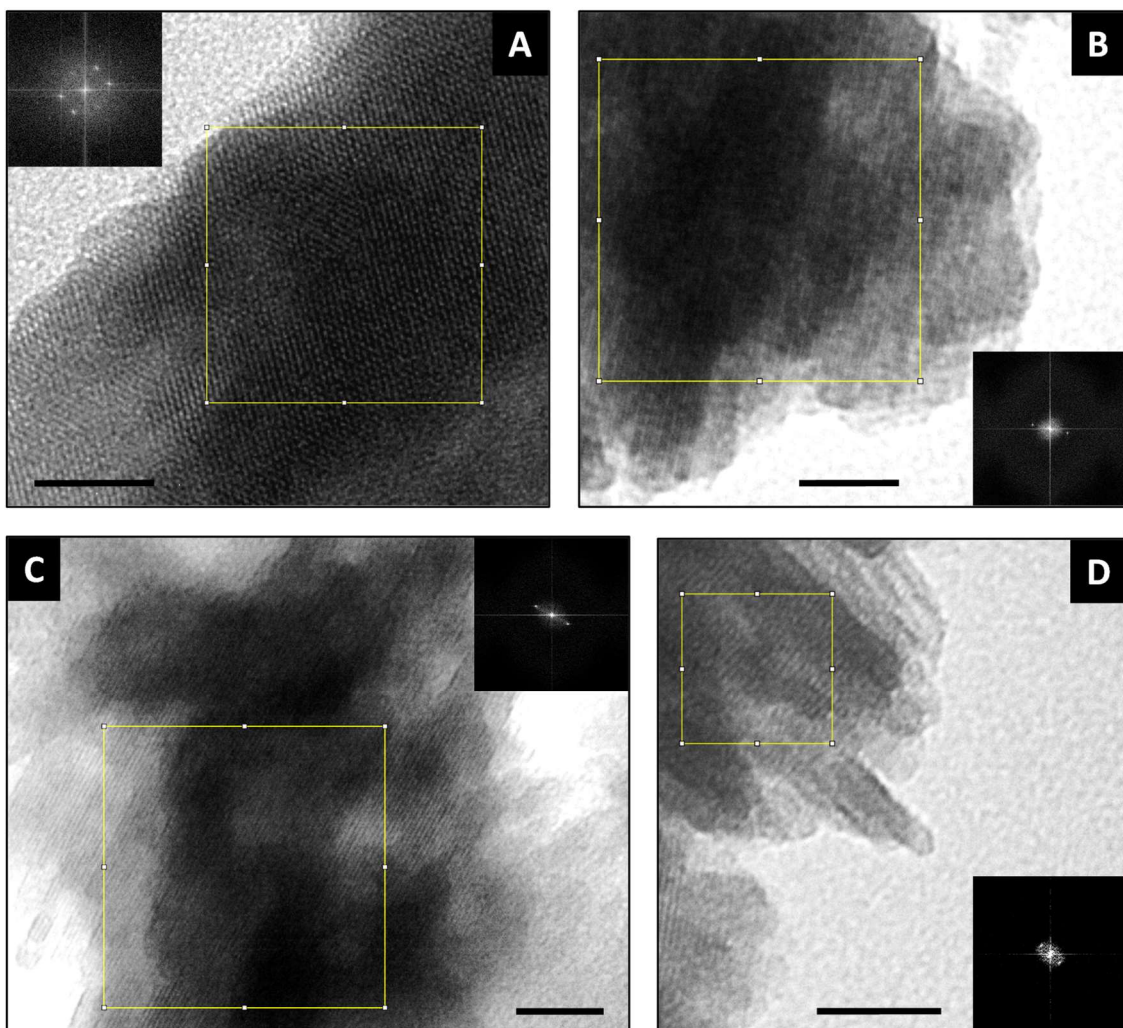


**Figure S6** TEM images of as-synthesized silicalite zeolites showing different crystallographic domains for varied initial TBA percentages: (A) 100.0 % TBA; (B) 98.0 % TBA; (C-D) 99.5 % TBA. The scale bars are 20 nm, and the black images are the FFT of the yellow squares' areas. In (C), the spacing between parallel planes takes a mean value of 1.07 nm ascribed to the distance between pentasil layers. In (D), the spacing between planes within the yellow square is 1.26 nm, very close to the value of the *c* cell parameter for MFI and MEL silicalites.

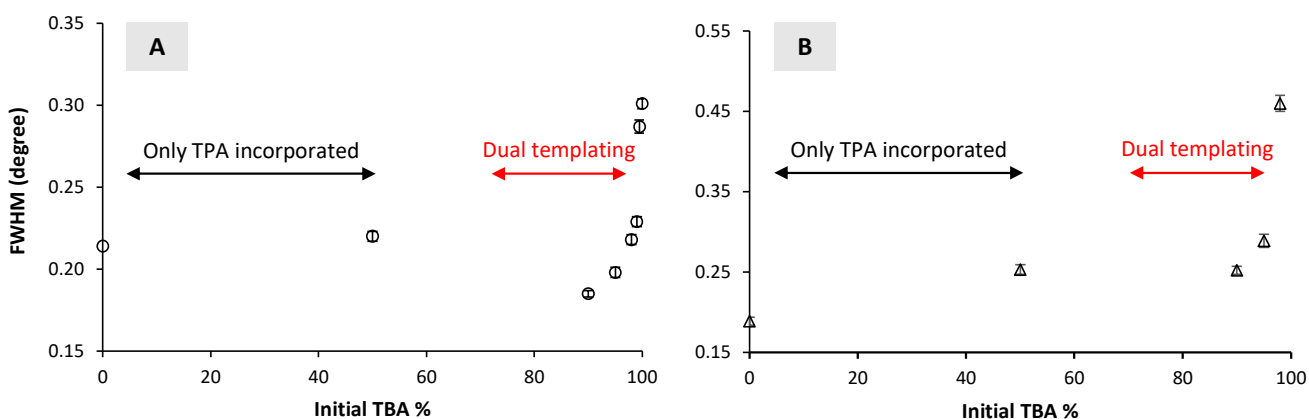


**Figure S7** FWHM evolutions for selected peaks as a function of initial TBA %: (A) Peak at ca. 7.9°; (B) Peak at ca. 24.5°.

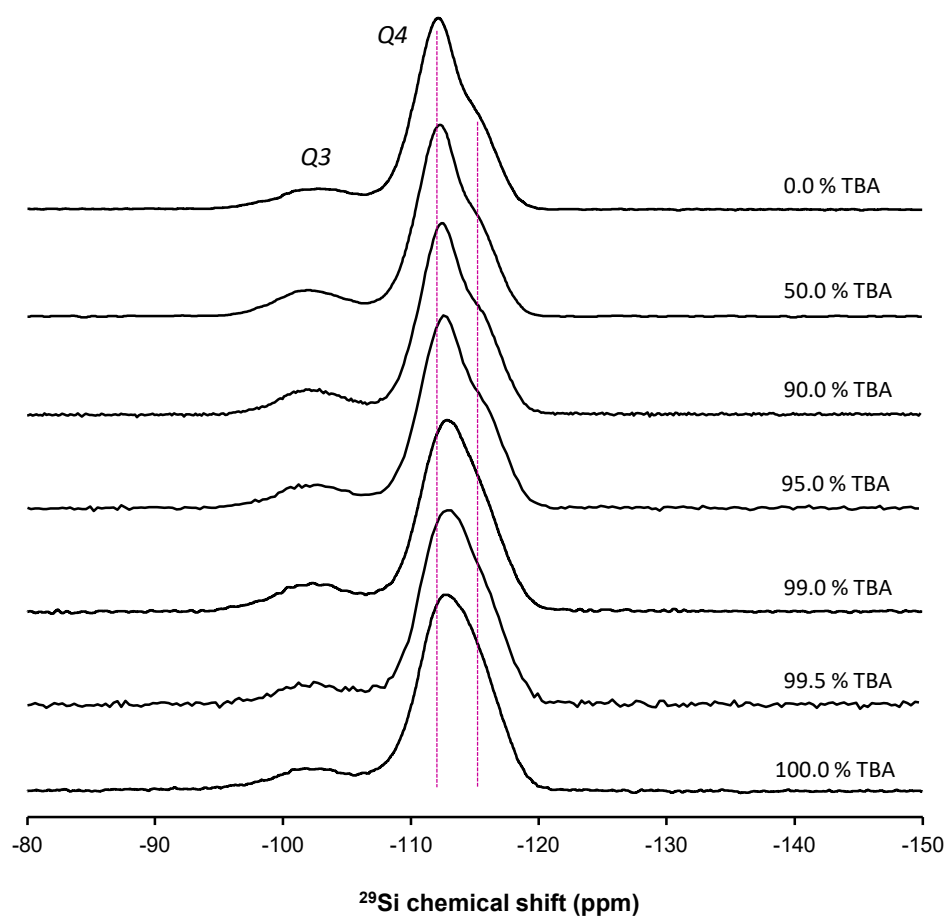


**Figure S8**  $^{29}\text{Si}\{^1\text{H}\}$  CP-MAS spectra ( $\nu_0[^{29}\text{Si}] = 79.5$  MHz,  $\nu_{\text{MAS}} = 5$  kHz) of as-synthesized silicalite zeolites. Percentages refer to initial TBA %.

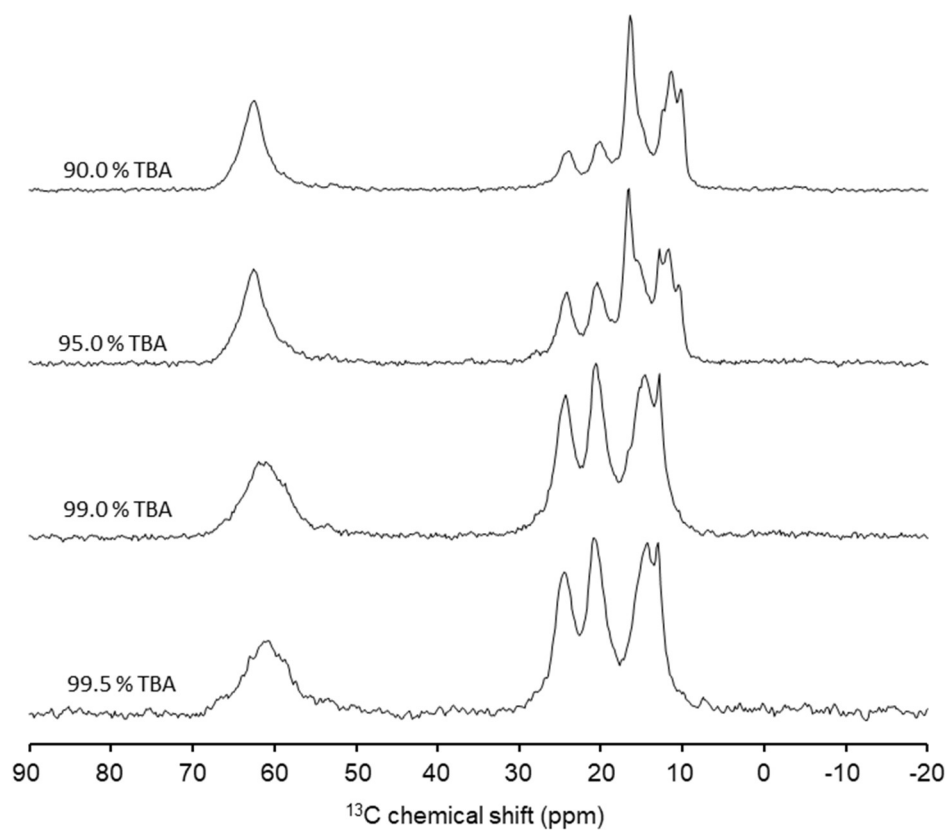


**Figure S9** Single-pulse  $^{13}\text{C}$  spectra ( $\nu_0[^{13}\text{C}] = 75.5 \text{ MHz}$ ,  $\nu_{\text{MAS}} = 5 \text{ kHz}$ ) of as-synthesized silicalite zeolites. Percentages refer to initial TBA %.

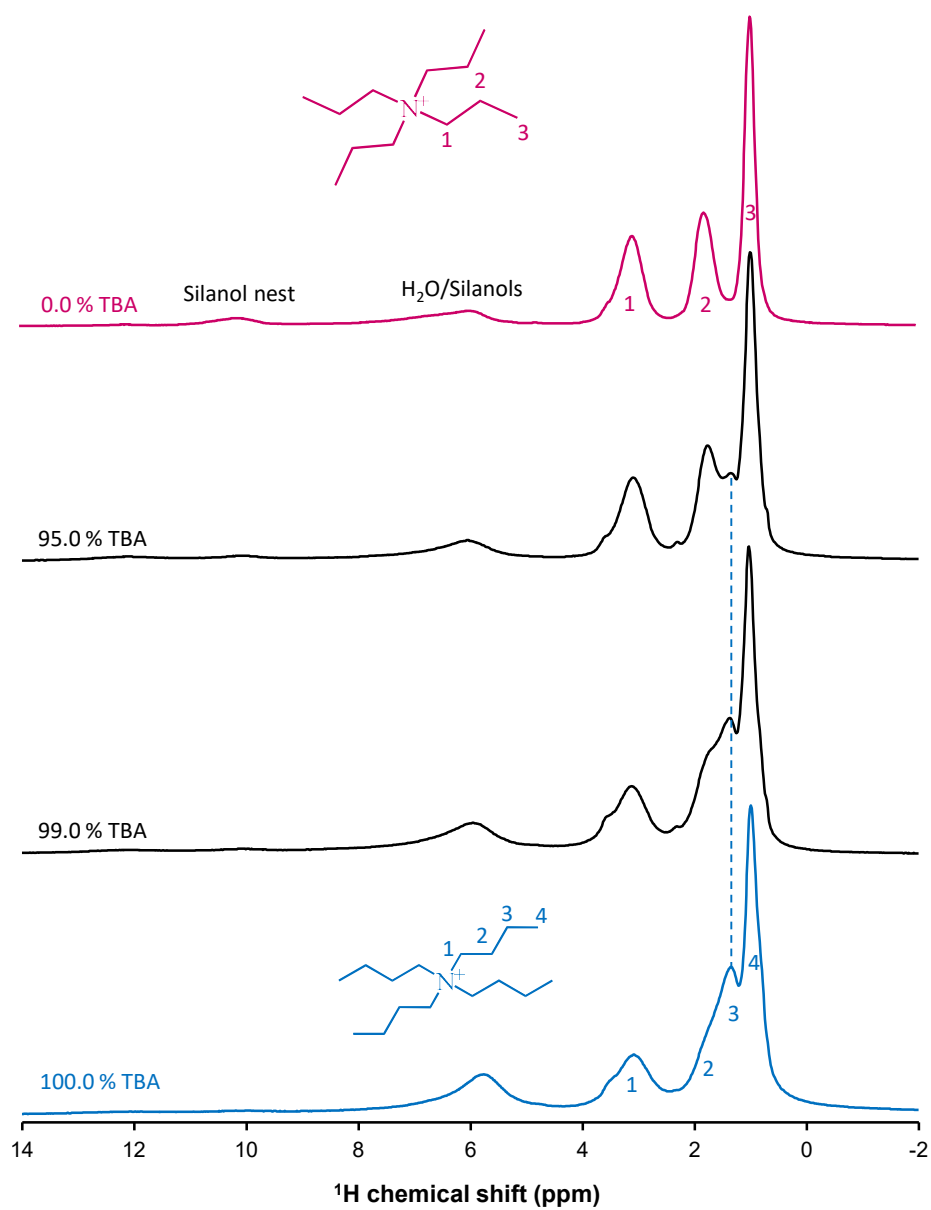


**Figure S10**  $^1\text{H}$  MAS spectra of as-synthesized silicalite zeolites recorded at very high magnetic field (20 T,  $\nu_0[{}^1\text{H}] \approx 850$  MHz) and MAS frequency (100 kHz). Percentages refer to initial TBA %.

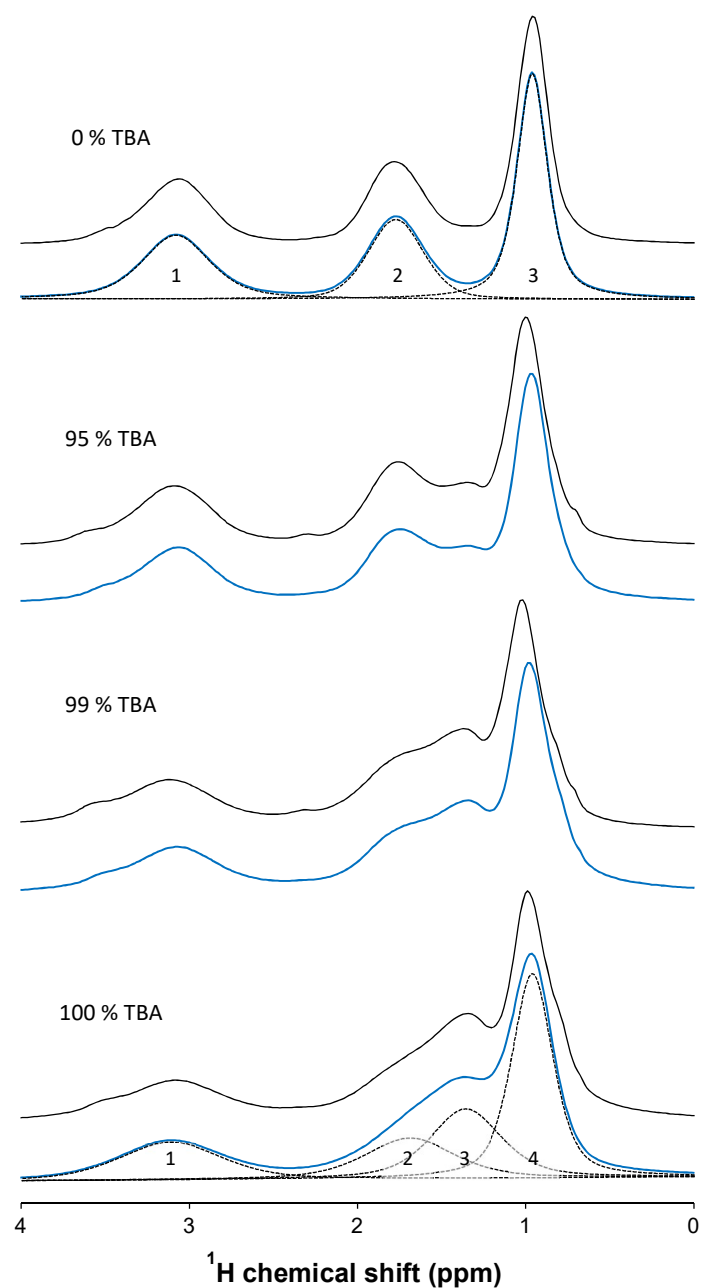


**Figure S11** Zoomed  $^1\text{H}$  NMR spectra of **Fig. S10** showing the OSDAs' resonances. Black lines correspond to experimental spectra. Blue lines correspond to models. For 0 and 100 % initial TBA, the models result from spectrum fitting (the individual contributions are represented as dotted lines and numbered following **Fig. S10**). For 95 and 99 % initial TBA, the models are obtained by a linear combination of 0 and 100 % spectra with weights taken from the relative proportions obtained by  $^{13}\text{C}$  NMR.

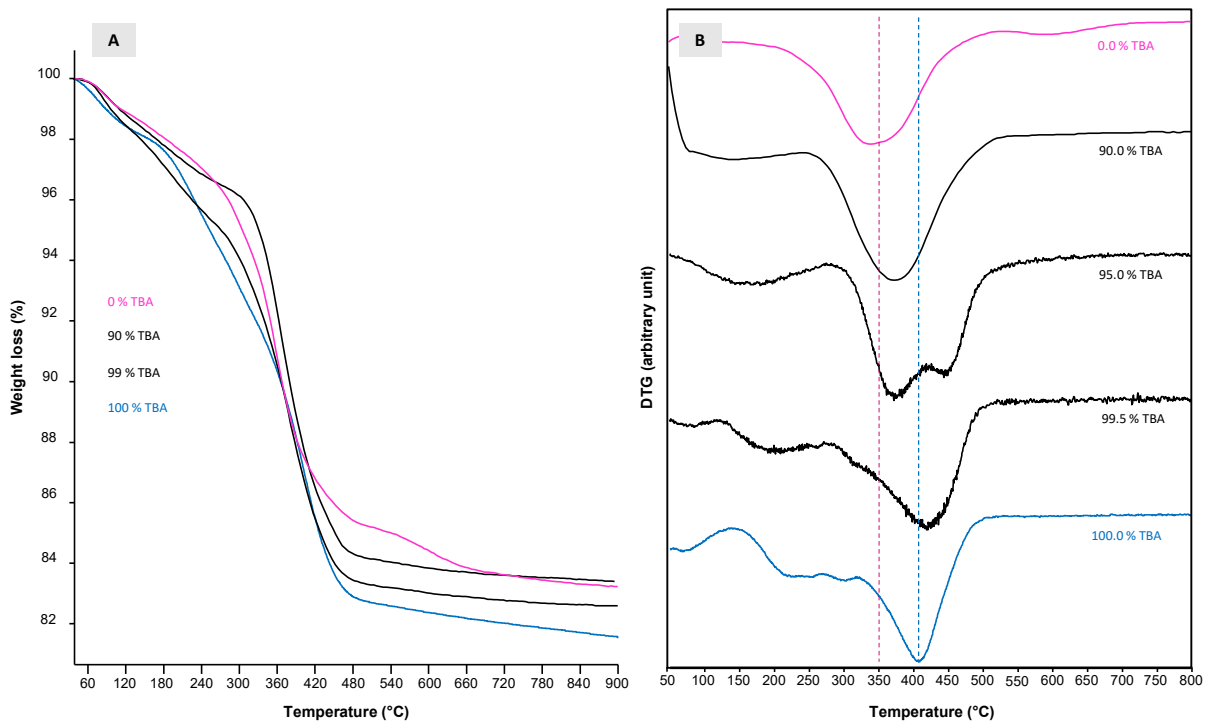


**Figure S12** TGA (A) and DTG (derivative thermogravimetry) (B) curves of of as-synthesized silicalite zeolites. Percentages refer to initial TBA %.

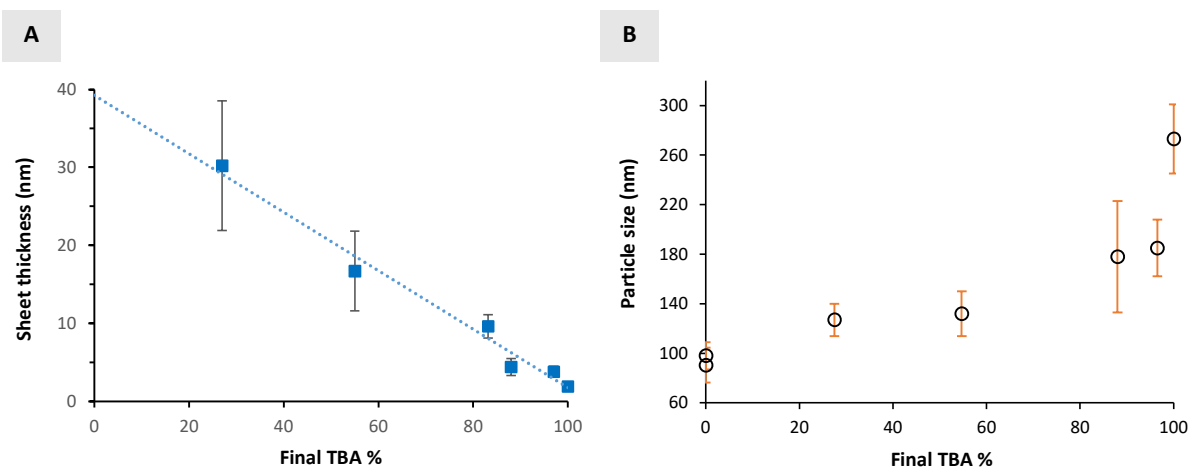


**Figure S13** Plots of sheet thickness (A) and particle size (B) of pure-silica zeolites as a function of TBA molar percentage in the OSDA incorporated in the final material. Errors bars correspond to  $\pm$  standard deviations.

**Table S2** Measured morphological parameters of the pure-silica samples synthesized with TPA and TBA OSDAs mixtures.

Initial molar TBA%	Final molar TBA%	Ave. particle size (nm) $\pm$ SD	Measurement no.	Ave. sheet thickness (nm) $\pm$ SD	Measurement no.
100	100	273 $\pm$ 28	148	1.9 $\pm$ 0.2	12
99.5	97	185 $\pm$ 23	27	3.8 $\pm$ 0.7	18
99	88	178 $\pm$ 45	16	4.4 $\pm$ 1.1	21
98	83 <sup>a</sup>	155 $\pm$ 18	188	9.6 $\pm$ 1.5	12
95	55	132 $\pm$ 18	25	16.7 $\pm$ 5.1	32
90	27	127 $\pm$ 13	64	30.2 $\pm$ 8.3	118
50	0	98 $\pm$ 11	59	-	-
0	0	90 $\pm$ 14	374	-	-

<sup>a</sup> Calculated value from the correlation in Fig. 3C.

## 5. Additional data on calcined zeolites

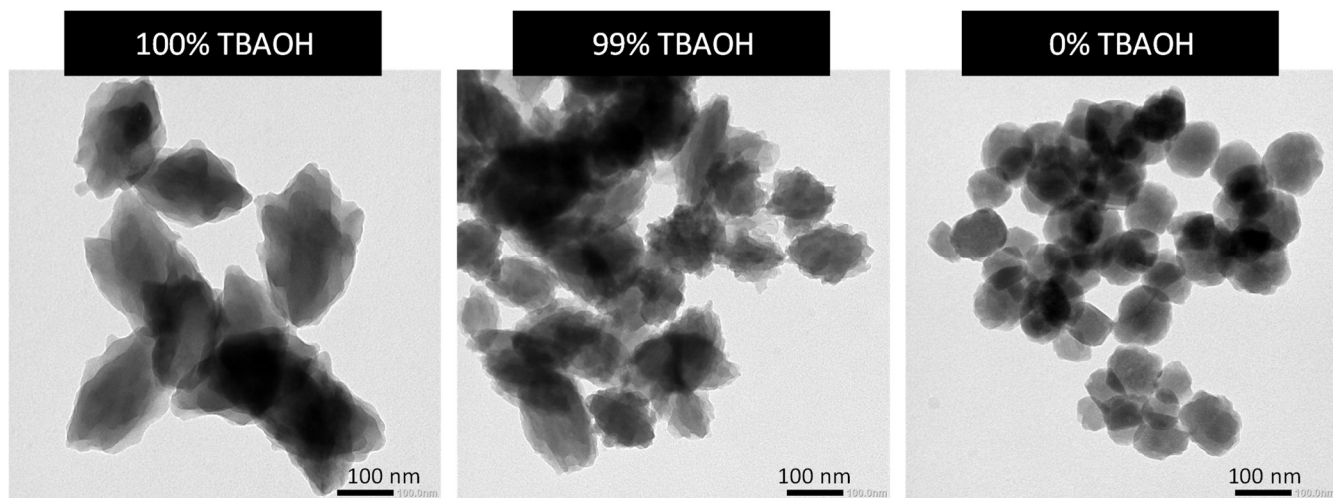


**Figure S14** TEM micrographs of calcined silicalite zeolites. Percentages refer to initial TBA %.

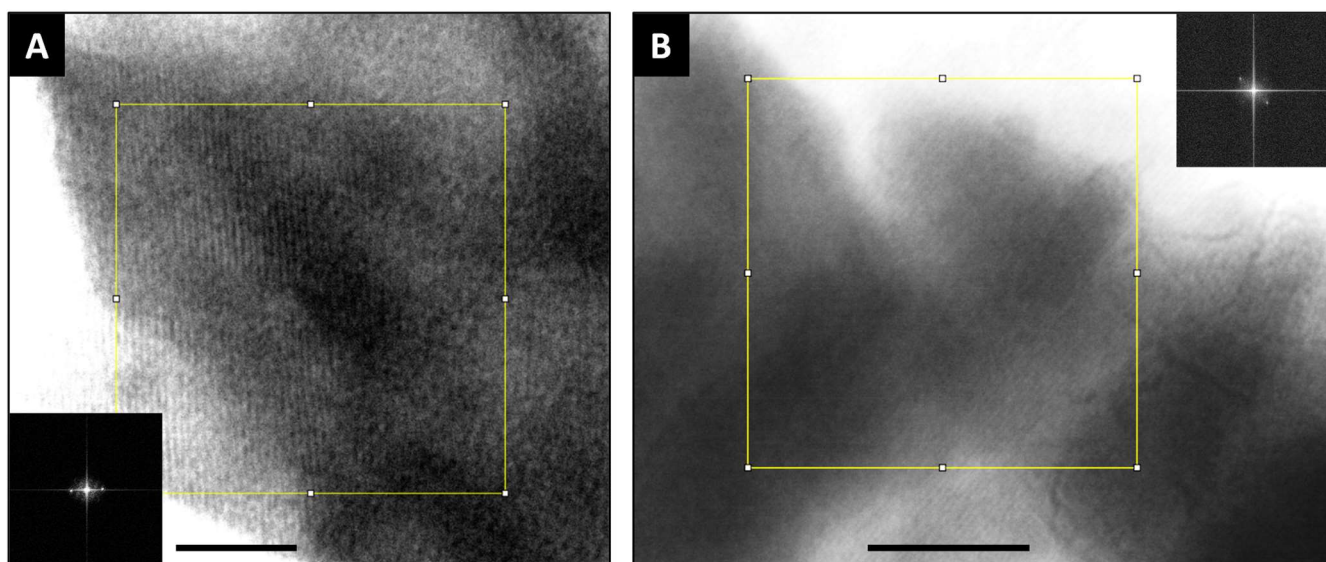


**Figure S15** TEM images of calcined silicalite zeolites showing different crystallographic domains for varied initial TBA percentages: (A) 100.0 % TBA; (B) 99.0 % TBA. The scale bars are 20 nm, and the black images are the FFT of the yellow squares' areas.

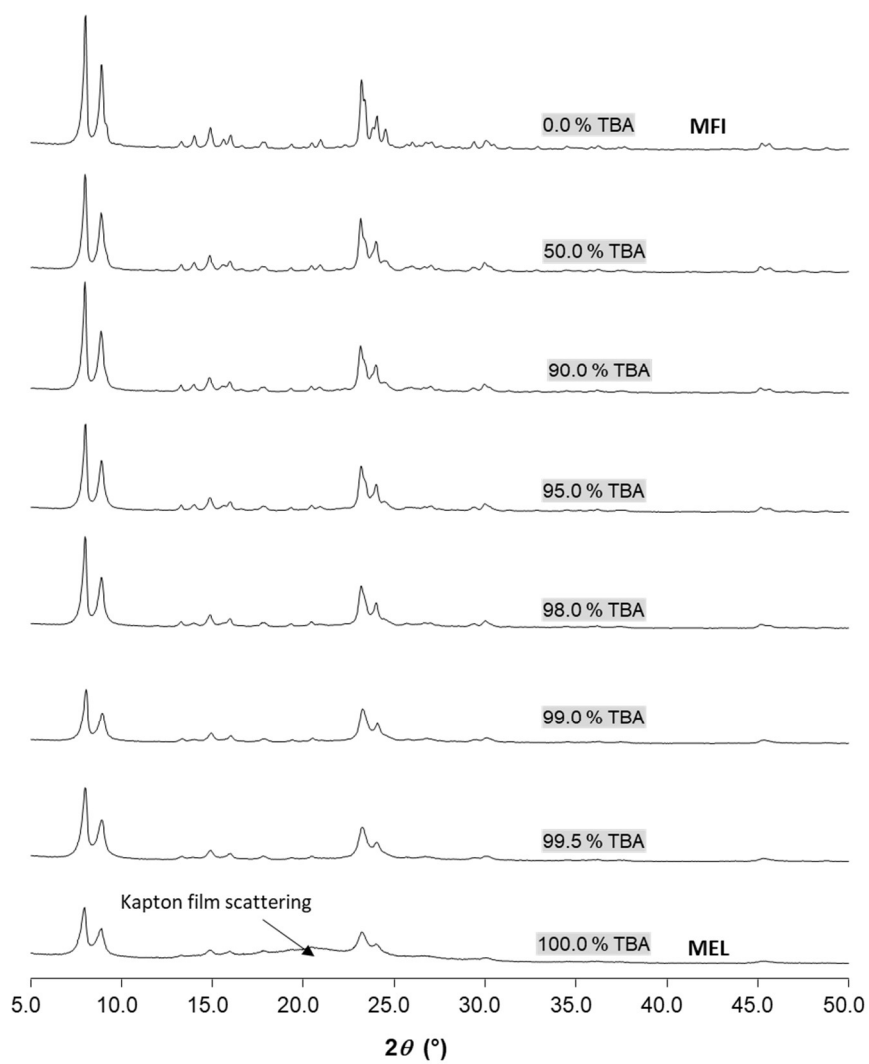


**Figure S16** XRD patterns of calcined silicalite zeolites. Percentages refer to initial TBA %.

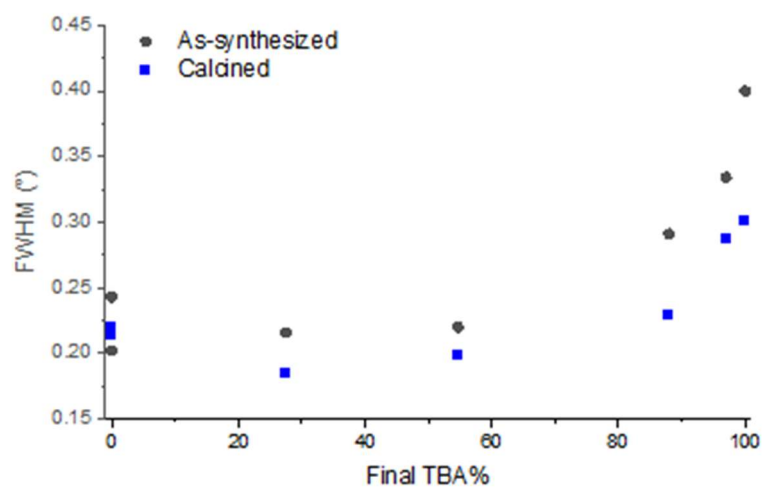


**Figure S17** Evolution of XRD FWHM for the peak at ca.  $7.9^\circ$ .

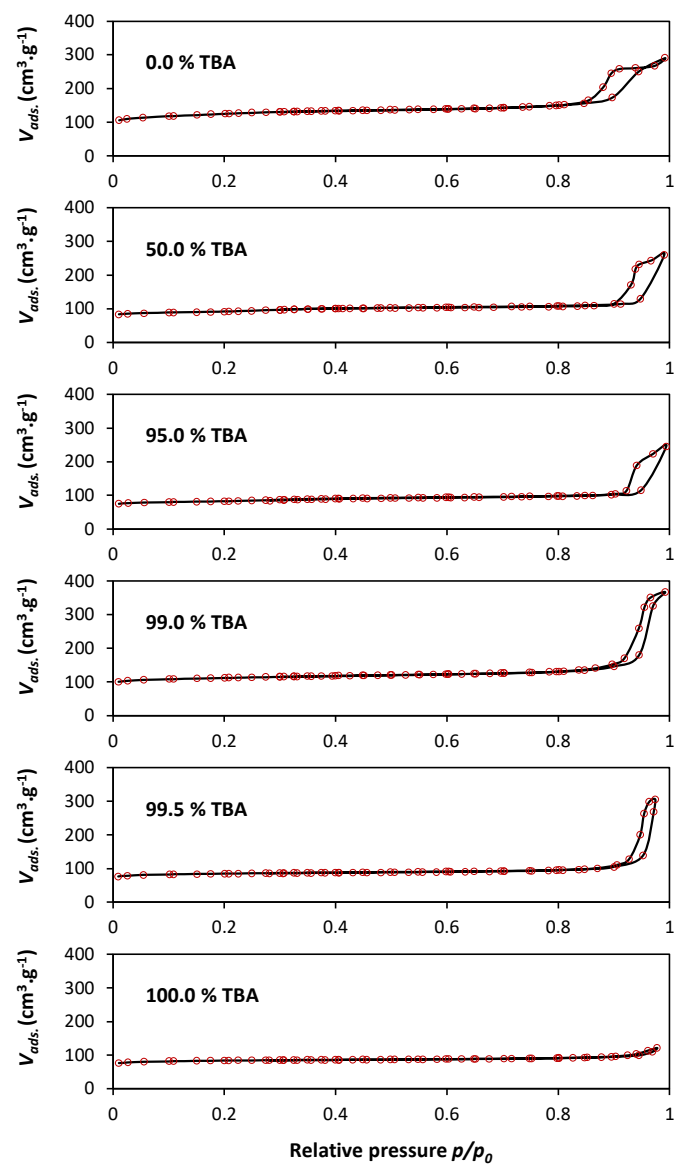


**Figure S18**  $N_2$  adsorption-desorption isotherms (77 K) of the calcined silicalite zeolites. Percentages refer to initial TBA %.

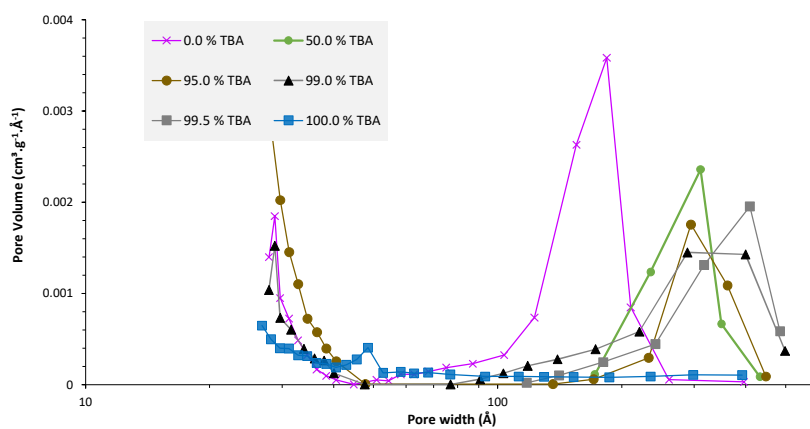


**Figure S19** BJH pore size distributions of the calcined silicalite zeolites. Percentages refer to initial TBA %.

## 6. Additional data for the Al-containing zeolites

**Table S3** Measured Si/Al and morphological parameters of the Al-containing zeolites.

Initial molar TBA%	Si/Al (XRF)	Ave. particle size (nm)	Measurement no.	Ave. sheet thickness (nm)	Measurement no.
100	43	230 ± 29	79	4.1 ± 1.0	20
99	39	172 ± 27	158	5.2 ± 1.2	68
0	76	150 ± 27	206	-	-

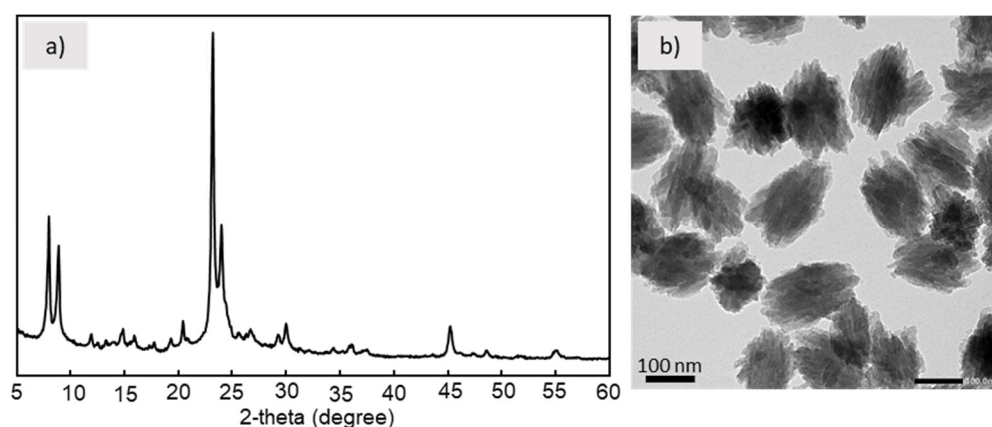


**Figure S20** a) XRD pattern of the Al-containing zeolite synthesized with 99 % TBA and b) its TEM image.

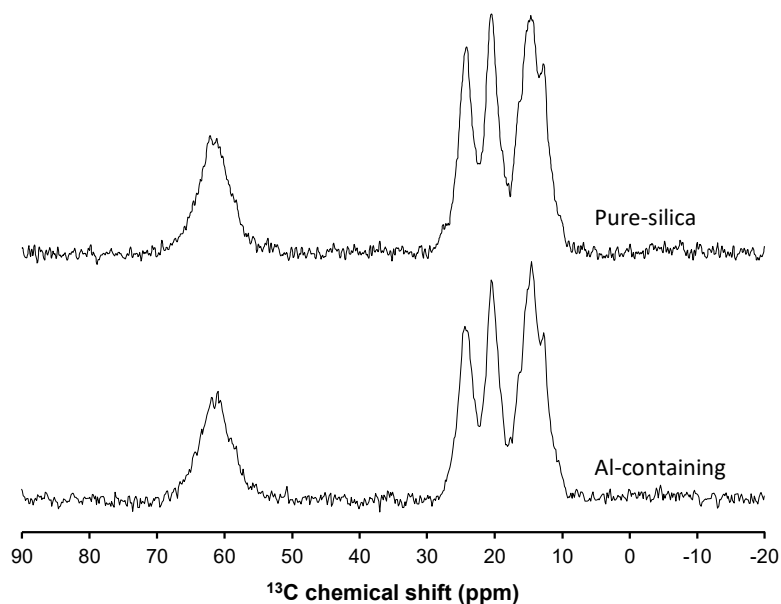


**Figure S21**  $^{13}\text{C}\{^1\text{H}\}$  CP-MAS spectra ( $\nu_0[^{13}\text{C}] = 75.5 \text{ MHz}$ ,  $\nu_{\text{MAS}} = 5 \text{ kHz}$ ) of pure-silica and Al-containing zeolite samples synthesized with 99 % TBA in the OSDA mixture.

## 7. ESI References

1. X. Zhang, D. Liu, D. Xu, S. Asahina, K. A. Cychosz, K. Varoon Agrawal, Y. AlWahedi, A. Bhan, S. A. Hashimi, O. Terasaki, M. Thommes and M. Tsapatsis, *Science*, 2012, **336**, 1684-1687.
2. C. A. Schneider, W. S. Rasband and K. W. Eliceiri, *Nat. Methods*, 2012, **9**, 671-675.
3. *ImageJ* program accessible via <https://imagej.net/software/imagej/>
4. J. H. de Boer, B. C. Lippens, B. G. Linsen, J. C. P. Broekhoff, A. van den Heuvel and T. J. Osinga, *J. Colloid Interface Sci.*, 1966, **21**, 405-414.
5. G. Jura and W. D. Harkins, *J. Chem. Phys.*, 1943, **11**, 430-431.
6. E. P. Barrett, L. G. Joyner and P. P. Halenda, *J. Am. Chem. Soc.*, 1951, **73**, 373-380.
7. G. Halsey, *J. Chem. Phys.*, 1948, **16**, 931-937.
8. D. Massiot, F. Fayon, M. Capron, I. King, S. Le Calvé, B. Alonso, J.-O. Durand, B. Bujoli, Z. Gan and G. Hoatson, *Magn. Reson. Chem.*, 2002, **40**, 70-76.
9. *Dmfit* program accessible via <https://nmr.cemhti.cnrs-orleans.fr/dmfit/>